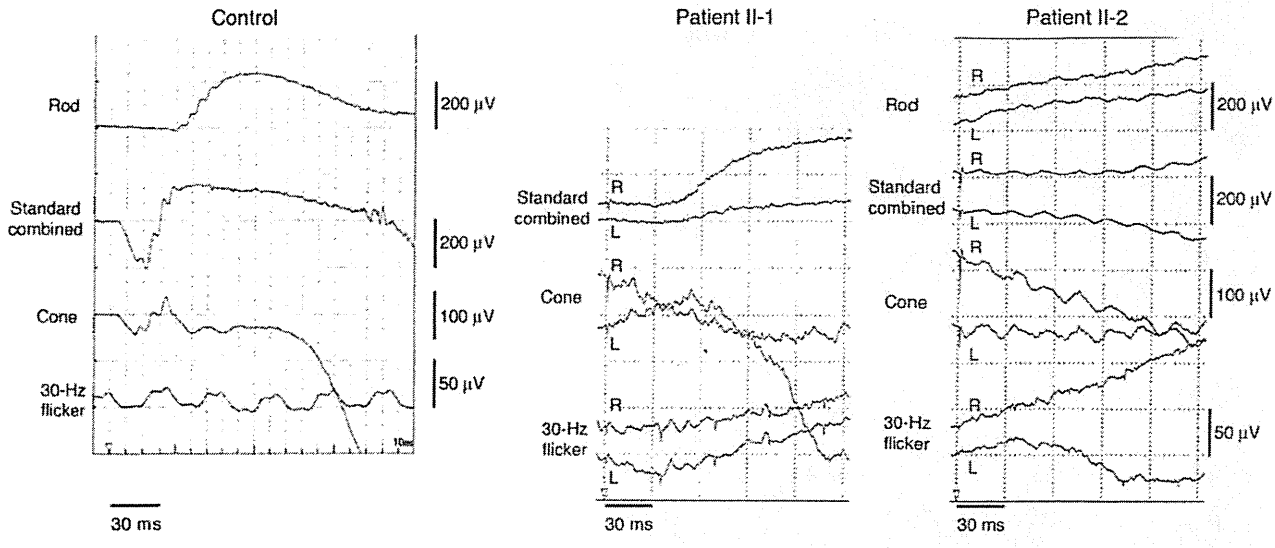

Figure 2. Full-field electroretinogram. The electroretinograms (ERGs; patient II-1) at the age of 9 years, showing no standard combined, photopic, or 30-Hz flicker responses in either eye. The ERGs (patient II-2) at the age of 7 years, showing no rod, standard combined, photopic, or 30-Hz flicker responses in either eye.

Clinical Electrophysiology of Vision. The procedure and conditions for ERG recording have been detailed previously [33].

Fasting venous blood samples were analyzed for glucose, lipid, lipoprotein, and hemogram levels and renal, liver, and thyroid function tests. In addition, hemoglobin A_{1c}, insulin, anti-thyroid peroxidase, anti-thyroglobulin antibodies, cortisol, luteinizing hormone, follicle stimulating hormone, testosterone, estradiol, prolactin, parathyroid hormone, and thyroid receptor antibody levels were examined. Chest X-rays and electrocardiograms were also performed.

DNA preparation and exome sequencing analysis: We obtained venous blood samples from the affected brothers and their unaffected parents. Genomic DNA was extracted from the blood samples by using a Gentra Puregene Blood kit (Qiagen, Tokyo, Japan) and sheared with a Covaris Ultrasonicator (Covaris, Woburn, MA). Construction of paired-end sequence libraries and exome capture were performed by using the Agilent Bravo automated liquid-handling platform with SureSelect XT Human All Exon kit V4 + UTRs kit (Agilent Technologies, Santa Clara, CA) according to the manufacturer's instructions. Enriched libraries were sequenced by using in Illumina HiSeq2000 sequencer (San Diego, CA), according to the manufacturer's instructions for 100-bp paired-end sequencing. Reads were mapped to the reference human genome (1000 genomes phase 2 reference, hs37d5) with Burrows–Wheeler Aligner software version 0.6.2 [34]. Duplicated reads were then removed by Picard MarkDuplicates module version 1.62, and mapped reads around insertion–deletion polymorphisms (INDELs) were realigned by using the Genome Analysis Toolkit (GATK) version 2.1–13 [35]. Base-quality scores were recalibrated by using GATK. Calling of mutations was performed by using the GATK UnifiedGenotyper module, and called single-nucleotide variants and INDELs were annotated by using snpEff software version 3.0 [36]. The mutations were annotated with the snpEff score ("HIGH," "MODERATE," or "LOW") and with the allele frequency in the 1000 genomes database. The mutations were then filtered so that only those with "HIGH" or "MODERATE" snpEff scores (indicating that the amino acid sequence would be functionally affected) and a frequency of less than 1% in the 1000 genome database were analyzed further. We also used new variations, which were not found in the in-house database of seven people exome data with control individuals without ocular diseases. Mutations were classified by hereditary information into homozygous recessive, heterozygous recessive, and de novo mutations in the family members. Filtered mutations were scored with PolyPhen software version 2.2.2 [37], which predicts the effect on the structure and function of the protein. The above exome analysis pipeline is available at Cell Innovation.

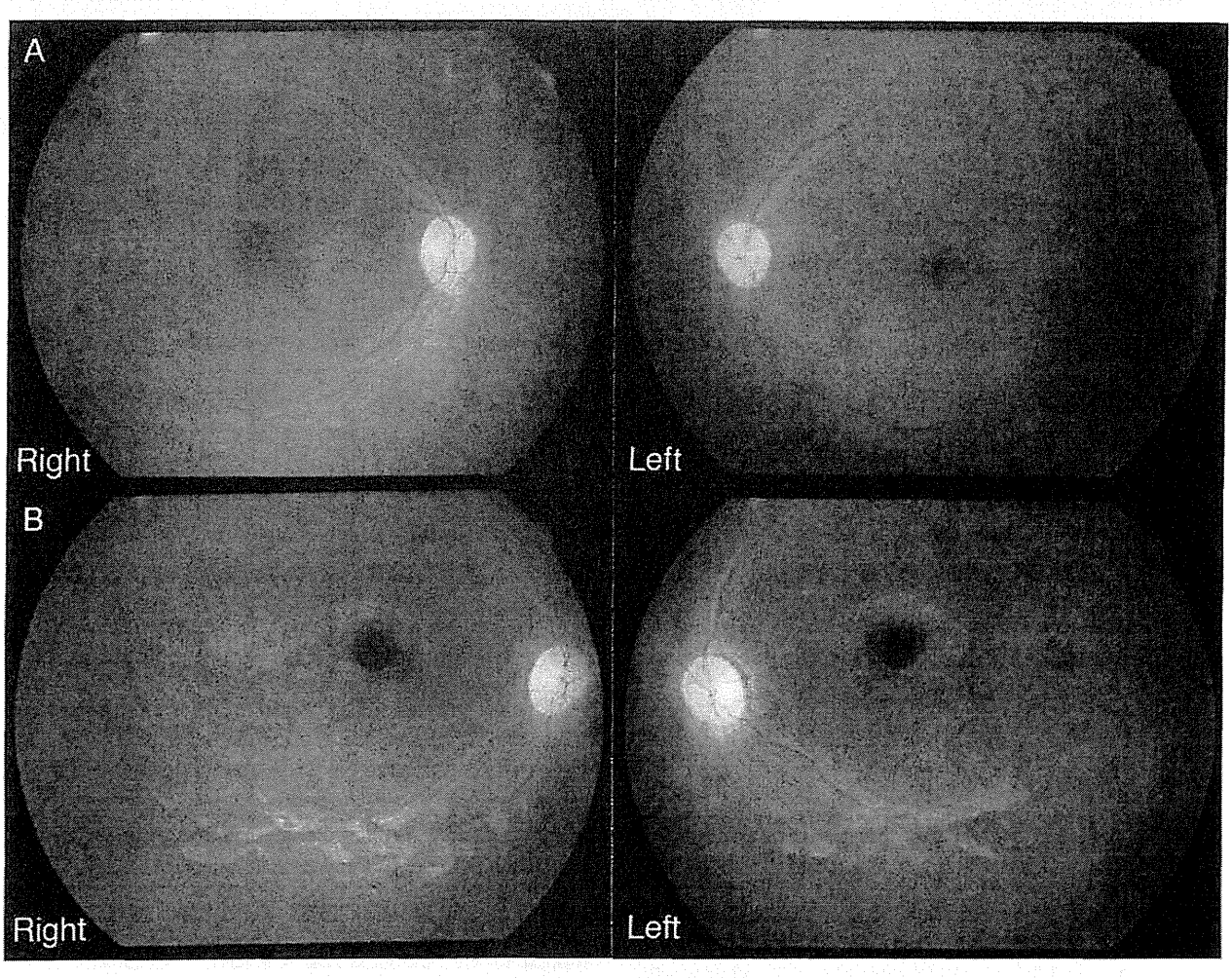

Figure 4. Fundus photographs of patients II-1 and II-2. **A** and **B**: Fundus photographs of patient II-1 at the age of 14 years (**A**) and patient II-2 at the age of 8 years (**B**) show retinal degeneration with attenuated vessels in the posterior poles of both eyes.

combined, photopic, or 30-Hz flicker responses in either eye (Figure 2). GP analysis at the age of 11 years showed markedly constricted visual fields in V-4e and I-4e isopters of both eyes (Figure 3A). The fundus photographs at the age of 14 years showed retinal degeneration with attenuated vessels from the arcade to the periphery in both eyes (Figure 4A). GP analysis at the age of 16 years showed more marked constricted visual fields of V-4e and I-4e isopters in both eyes than those observed at the age of 11 years (Figure 3B); a similar analysis at the age of 22 years showed a small visual field of V-4e isopter in the right eye and no visual field in the left eye (Figure 3C). TD-OCT at the age of 22 years showed total macular thinning in both eyes (Figure 5A). At the age of 29 years, his BCVA was light perception (LP) in the right eye and no light perception in the left eye. Intraocular pressure in each eye was within the normal range. He had severe cortical and subcapsular cataracts in the right (Figure 6) and left eyes, and the fundi were not visible due to these cataracts.

Ophthalmologic findings for patient II-2: Patient II-2, the younger of the two brothers, visited our hospital at the age of 2 years and 6 months with the main complaint of poor visual acuity and photophobia. At the age of 3 years, his BCVA was 0.01 (+1.50 dpt) in the right eye and 0.01 (+1.50 dpt) in the left eye. Fundus examination showed retinal degeneration with slight attenuation of peripheral vessels. At the age of 4 years, he failed the Ishihara test. At the age of 6 years, the panel D-15 test showed irregular arrangements along no particular axis, and the GP could not be measured well because of low visual acuity and nystagmus. The ERG at the age of 7 years showed no rod, standard combined, photopic, or 30-Hz flicker responses in either eye (Figure 2). The fundus examination at

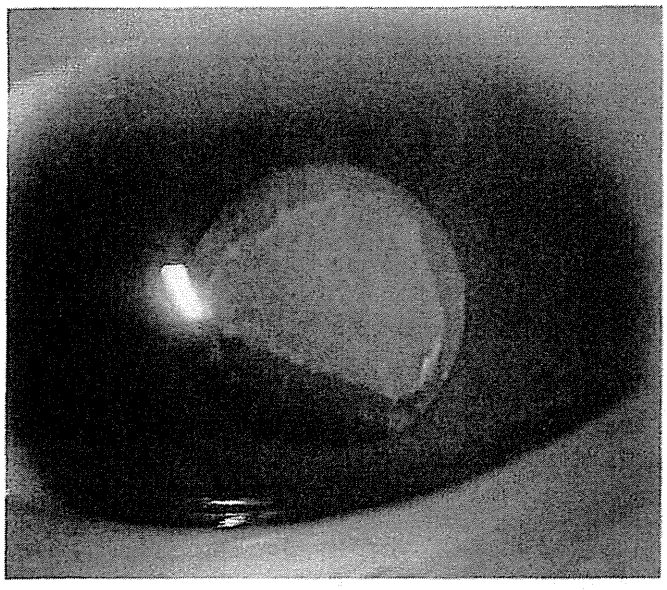

Figure 6. Anterior segment of the right eye in patient II-1. A severe cortical and anterior subcapsular cataract is present at the age of 29 years.

Systemic features except ocular findings: Systemic examinations were performed for patient II-1 at the age of 29 and patient II-2 at the age of 23. Both patients had hepatic dysfunction, hyperlipidemia, hypogonadism, short stature, and flat feet, and neither patient had hearing loss, renal failure, abnormal digits, history of developmental delay, mental retardation, scoliosis, hypertension, or alopecia. Obesity was present in patient II-1 only. Patient II-1 had T2DM, whereas patient II-2 showed hyperinsulinemia. Subclinical hypothyroidism was diagnosed in patient II-2 only. Recurrent pulmonary infections were not observed, and chest X-rays showed neither fibrotic infiltrations nor cardiac dilation in either patient. Infantile asthma was experienced by both patients. Electrocardiogram analysis showed no arrhythmia in either patient. Summaries of the clinical features, bio-information, and detailed laboratory data are presented in Table 1 and Table 2. Collectively, the phenotypes of the brothers were consistent with those described for AS.

Exome sequencing analysis and identification of a gene mutation: We performed whole-exome sequencing of the two affected brothers and their parents by using the Agilent SureSelect Human All Exon kit followed by Illumina HiSeq 2000 platforms. Sequences of average length 11.8 Gb were generated from 101-bp paired-end sequences. After eliminating reads from PCR duplicates by discarding reads with duplicated start sites, we achieved 58-fold depth and 87% coverage in Refseq annotated regions (Table 3). When the sequences were compared with the reference human genome (hs37d5), 3,506,741 mutations were found in the two brothers and their parents (Table 4). To distinguish potentially causal mutations from other mutations, we focused only on mutations that could change the amino acid sequence (19,574 mutations), such as nonsynonymous mutations, splice acceptor and donor site mutations, and INDELs. We also assumed the frequency of the mutations responsible for AS is likely to be under 1%. After filtering with snpEff score and frequency criteria, we filtered the remaining 3,685 mutations by using the pattern of inheritance and identified 17 gene mutations as causal candidates. Among these mutations, nine mutations were found homozygous in the HECT domain containing E3 ubiquitin protein ligase 3 (*HECTD3*), the vitrin (*VIT*), the protein kinase domain containing, cytoplasmic (*PKDCC*), the ATP-binding cassette, sub-family G (*WHITE*), member 8 (*ABCG8*), the leucine-rich pentatricopeptide repeat containing (*LRPPRC*), the G protein-coupled receptor 75 (*GPR75*), the notochord homeobox (*NOTO*), the matrix-remodelling associated 5 (*MXRA5*), and the *ALMS1* genes. Eight mutations were found as compound heterozygous mutations within the PERP, TP53 apoptosis effector (*PERP*), the transforming, acidic coiled-coil containing protein 2 (*TACC2*), the zinc finger protein, FOG family member 1 (*ZFPM1*), and the lipoxygenase homology domains 1 (*LOXHD1*) genes. No de novo mutations were found. To determine the causative gene, we investigated SAGE (EyeSAGE) database to determine if the candidate genes are expressed in the retina. Nine candidate mutations were identified within *VIT, LRPPRC, PERP, TACC2, ZFPM1,* and *ALMS1* genes. These nine candidate genes were further reduced by the BIOBASE Biologic Database and RetNet to determine which of the candidate genes would be likely to

Molecular Vision 2013; 19:2393-2406 <http://www.molvis.org/molvis/v19/2393>

Table 2. Bio-information and biochemical assessment

Bio-information and blood test results	Normal range	Patient II-1	Patient II-2
Bio-information			
Weight (kg)		60	52
Height (m)		1.52	1.55
Body mass index (kg/m^2)	18.5–25	**25.96**	21.6
Biochemical assessment			
Fasting blood glucose (mg/dl)	65–109	**247**	77
Hemoglobin A1c (%)	4.6–6.2	**12.5**	6.0
Urea (mg/dl)	8–20	16	10
Creatinine (mg/dl)	0.50–1.10	0.99	0.63
Uric acid (mg/dl)	3.1–6.9	4.2	3.6
Sodium (mmol/l)	136–146	140	141
Potassium (mmol/l)	3.6–4.8	4.1	4.3
Chloride (mmol/l)	98–109	100	104
Calcium (mg/dl)	8.6–10.2	**10.3**	10.2
Aspartate aminotransferase (U/l)	10–33	**76**	**81**
Alanine aminotransferase (U/l)	6–35	**99**	**241**
Gamma glutamyl transpeptidase (U/l)	12–65	**134**	**135**
Alkaline phosphatase (U/l)	96–300	285	**319**
Low density lipoprotein-cholesterol (mg/dl)	70–139	120	**282**
Total cholesterol (mg/dl)	120–219	211	**441**
Triglycerides (mg/dl)	30–149	**309**	**761**
Albumin/globulin (g/dl)	3.5–5.2	5.0	5.1
Hemogram			
White blood cells (10^3/ml)	3.3–8.6	4.7	6.4
Red blood cells (10^6/ml)	4.10–5.50	5.00	4.88
Hemoglobin (g/dl)	13.5–16.5	14.0	14.3
Hematocrit (%)	40.0–50.0	42.3	42.7
Mean corpuscular volume (fl)	83.0–101.0	84.6	87.5
Platelets (10^3/ml)	150–350	166	251
Erythrocyte sedimentation rate (mm/h)	2–10	21	19
Hormones and autoantibodies			
Free T3 (pg/ml)	2.36–5.00	**2.34**	2.47
Free T4 (pmol/l)	0.88–1.67	1.33	**0.79**

Table 3. DNA sequence statistics

Family members	Read length (bp)	Number of reads	Mapping rate (%)	Mean depth (fold)	Coverage (%)
II-2 (younger brother)	101	47,724,724	99.4	46.6	88.5
II-1 (elder brother)	101	68,584,852	99.4	59.6	86.1
I-1 (father)	101	57,103,807	99.3	69.3	88.5
I-2 (mother)	101	59,776,264	99.3	56.8	86
Average	101	58,297,412	99.3	58.1	87.3

or anatomic changes of the retina [14,18,21,40] have been reported. For instance, a study of the pathology of the retina of a 2-year-old girl with AS showed hypocellularity of the ganglionic cell layer, the inner nuclear layer, and the outer nuclear layer (ONL) in addition to an absence of rod and cone outer segments and disruption of retinal pigment epithelium [18,21]; a study of a 42-year-old female with AS revealed severe reduction of all retinal layers containing a complete lack of photoreceptors and deposits of melanin pigments in the inner nuclear layer [14]; and OCT findings of a 5-year-old boy with AS showed only a slight thinning of the central retina [40]. In our patients, OCT findings showed marked retinal thinning (Figure 5A,B). The retinal layers of patient II-2 could not be distinguished because of marked retinal thinning (Figure 5C).

A study using retinal sections of *Almsl* knockout (*Almsl*$^{-/-}$) mice showed loss of the cell bodies in the ONL, shortening of the inner and outer segments, and incorrect localization of rhodopsin to the ONL [7]. The mislocalization of rhodopsin in the *Almsl*$^{-/-}$ mice indicates a defective rhodopsin transport system through the photoreceptor-connecting cilium [7]. The connecting cilium, damaged by loss of function of ALMS1, modifies the outer segments of the photoreceptors. Therefore, it has been suggested that defective protein transport across the connecting cilium is the probable cause of early onset severe retinal degeneration in AS patients [10]. We consider that the marked retinal thinning (Figure 5) and loss of retinal function (Figure 2) observed in our patients are due to a defective transport system across the photoreceptor-connecting cilium, resulting from the homozygous truncated mutation (p.Q2051X).

Variability in the phenotypic expression of AS is observed within sets of affected siblings [14,41–43]. Most patients with AS eventually develop T2DM, although there is wide variability in the age of onset [14]. Here, patient II-1 showed T2DM, but patient II-2 exhibited hyperinsulinemia, a predictor of T2DM (Table 2), suggesting that he might develop T2DM in the future. In addition, patient II-2 showed subclinical hypothyroidism, whereas patient II-1 did not exhibit hypothyroidism (Table 2). Hypothyroidism or subclinical hypothyroidism is reported to exist in approximately 20% of AS patients [14,19]. Most clinical features, such as retinal degeneration, hepatic dysfunction, hyperlipidemia, hypogonadism, short stature, and wide feet, were common features of the affected brothers (Table 1, Table 2); however, slight phenotypic differences in terms of glucose tolerance and thyroid function were observed between them.

ALMS1 protein has several notable sequence features, including an extensive tandem repeat domain (34×47 amino acid approximate tandem repeat, residues 538–2,199), a putative leucine-zipper motif (residues 2,480–2,501), and an ALMS motif (residues 4,035–4,167). Although the precise roles of the above domain and motifs are unknown, it is suggested that two regions of ALMS1—a relatively small internal region (residues 2,261–2,602) and a larger C-terminal region (residues 3,176–4,169)—play important

Table 4. Number of mutations after each filtering step

Filtering step	Number of mutations
1. Raw single-nucleotide variants plus *insertion–deletion* polymorphisms	3,506,741
2. Mutations capable of changing amino acid sequence	19,574
3. Mutations filtering by the snpEff score and existing at a frequency of less than 1% in 1000 genomes	3,685
4. Mutations filtering by the pattern of inheritance	17
5. Mutations expressed in retina, confirmed by SAGE database[a]	9
6. Mutations narrowed down using BIOBASE Biologic Database[b] and RetNet database[c]	1

[a]SAGE: serial analysis of gene expression;[b]BIOBASE Biologic Database (EyeSAGE); [c]RetNet database.

13. Marshall JD, Hinman EG, Collin GB, Beck S, Cerqueira R, Maffei P, Milan G, Zhang W, Wilson DI, Hearn T, Tavares P, Vettor R, Veronese C, Martin M, So WV, Nishina PM, Naggert JK. Spectrum of *ALMS1* variants and evaluation of genotype-phenotype correlations in Alström syndrome. Hum Mutat 2007; 28:1114-23. [PMID: 17594715].

14. Marshall JD, Bronson RT, Collin GB, Nordstrom AD, Maffei P, Paisey RB, Carey C, Macdermott S, Russell-Eggitt I, Shea SE, Davis J, Beck S, Shatirishvili G, Mihai CM, Hoeltzenbein M, Pozzan GB, Hopkinson I, Sicolo N, Naggert JK, Nishina PM. New Alström syndrome phenotypes based on the evaluation of 182 cases. Arch Intern Med 2005; 165:675-83. [PMID: 15795345].

15. Koç E, Bayrak G, Suher M, Ensari C, Aktas D, Ensari A. Rare case of Alström syndrome without obesity and with short stature, diagnosed in adulthood. Nephrology (Carlton) 2006; 11:81-4. [PMID: 16669965].

16. Akdeniz N, Bilgili SG, Aktar S, Yuca S, Calka O, Kilic A, Kosem M. Alström syndrome with acanthosis nigricans: a case report and literature review. Genet Couns 2011; 22:393-400. [PMID: 22303800].

17. Dyer DS, Wilson ME, Small KW, Pai GS. Alström syndrome: a case misdiagnosed as Bardet-Biedl syndrome. J Pediatr Ophthalmol Strabismus 1994; 31:272-4. [PMID: 7807310].

18. Russell-Eggitt IM, Clayton PT, Coffey R, Kriss A, Taylor DS, Taylor JF. Alström syndrome. Report of 22 cases and literature review. Ophthalmology 1998; 105:1274-80. [PMID: 9663233].

19. Marshall JD, Beck S, Maffei P, Naggert JK. Alström syndrome. Eur J Hum Genet 2007; 15:1193-202. [PMID: 17940554].

20. Lambert SR, Kriss A, Taylor D, Coffey R, Pembrey M. Follow-up and diagnostic reappraisal of 75 patients with Leber's congenital amaurosis. Am J Ophthalmol 1989; 107:624-31. [PMID: 2658617].

21. Russell-Eggitt IM, Taylor DS, Clayton PT, Garner A, Kriss A, Taylor JF. Leber's congenital amaurosis--a new syndrome with a cardiomyopathy. Br J Ophthalmol 1989; 73:250-4. [PMID: 2713302].

22. Ikeda Y, Morita Y, Matsuo Y, Akanuma Y, Itakura H. A case of Alström syndrome associated with situs inversus totalis and characteristic liver cirrhosis. Nippon Naika Gakkai Zasshi 1974; 63:1303-11. [PMID: 4477178].

23. Awazu M, Tanaka T, Sato S, Anzo M, Higuchi M, Yamazaki K, Matsuo N. Hepatic dysfunction in two sibs with Alström syndrome: case report and review of the literature. Am J Med Genet 1997; 69:13-6. [PMID: 9066877].

24. Awazu M, Tanaka T, Yamazaki K, Kato S, Higuchi M, Matsuo N. A 27-year-old woman with Alström syndrome who had liver cirrhosis. Keio J Med 1995; 44:67-73. [PMID: 7658647].

25. Shendure J, Ji H. Next-generation DNA sequencing. Nat Biotechnol 2008; 26:1135-45. [PMID: 18846087].

26. Mardis ER. The impact of next-generation sequencing technology on genetics. Trends Genet 2008; 24:133-41. [PMID: 18262675].

27. Mardis ER. Next-generation DNA sequencing methods. Annu Rev Genomics Hum Genet 2008; 9:387-402. [PMID: 18576944].

28. Ansorge WJ. Next-generation DNA sequencing techniques. New Biotechnol 2009; 25:195-203. [PMID: 19429539].

29. Teer JK, Mullikin JC. Exome sequencing: the sweet spot before whole genomes. Hum Mol Genet 2010; 19:R2R145-51. [PMID: 20705737].

30. Li Y, Vinckenbosch N, Tian G, Huerta-Sanchez E, Jiang T, Jiang H, Albrechtsen A, Andersen G, Cao H, Korneliussen T, Grarup N, Guo Y, Hellman I, Jin X, Li Q, Liu J, Liu X, Sparso T, Tang M, Wu H, Wu R, Yu C, Zheng H, Astrup A, Bolund L, Holmkvist J, Jorgensen T, Kristiansen K, Schmitz O, Schwartz TW, Zhang X, Li R, Yang H, Wang J, Hansen T, Pedersen O, Nielsen R, Wang J. Resequencing of 200 human exomes identifies an excess of low-frequency non-synonymous coding variants. Nat Genet 2010; 42:969-72. [PMID: 20890277].

31. Kim DW, Nam SH, Kim RN, Choi SH, Park HS. Whole human exome capture for high-throughput sequencing. Genome 2010; 53:568-74. [PMID: 20616878].

32. Hodges E, Rooks M, Xuan Z, Bhattacharjee A, Benjamin Gordon D, Brizuela L, Richard McCombie W, Hannon GJ. Hybrid selection of discrete genomic intervals on custom-designed microarrays for massively parallel sequencing. Nat Protoc 2009; 4:960-74. [PMID: 19478811].

33. Takeuchi T, Hayashi T, Bedell M, Zhang K, Yamada H, Tsuneoka H. A novel haplotype with the R345W mutation in the EFEMP1 gene associated with autosomal dominant drusen in a Japanese family. Invest Ophthalmol Vis Sci 2010; 51:1643-50. [PMID: 19850834].

34. Li H, Durbin R. Fast and accurate short read alignment with Burrows-Wheeler transform. Bioinformatics 2009; 25:1754-60. [PMID: 19451168].

35. McKenna A, Hanna M, Banks E, Sivachenko A, Cibulskis K, Kernytsky A, Garimella K, Altshuler D, Gabriel S, Daly M, DePristo MA. The Genome Analysis Toolkit: a MapReduce framework for analyzing next-generation DNA sequencing data. Genome Res 2010; 20:1297-303. [PMID: 20644199].

36. Cingolani P, Platts A, Wang le L, Coon M, Nguyen T, Wang L, Land SJ, Lu X, Ruden DM. A program for annotating and predicting the effects of single nucleotide polymorphisms, SnpEff: SNPs in the genome of Drosophila melanogaster strain w1118; iso-2; iso-3. Fly (Austin) 2012; 6:80-92. [PMID: 22728672].

37. Adzhubei I, Jordan DM, Sunyaev SR. Predicting functional effect of human missense mutations using PolyPhen-2. Curr Protoc Hum Genet 2013; Chapter 7:Unit7 20.

38. Green JS, Parfrey PS, Harnett JD, Farid NR, Cramer BC, Johnson G, Heath O, McManamon PJ, O'Leary E, Pryse-Phillips W. The cardinal manifestations of Bardet-Biedl syndrome, a form of Laurence-Moon-Biedl syndrome. N Engl J Med 1989; 321:1002-9. [PMID: 2779627].

Clinical Ophthalmology Dove

CASE REPORT

Two siblings with late-onset cone–rod dystrophy and no visible macular degeneration

Hiroyuki Sakuramoto[1]
Kazuki Kuniyoshi[1]
Kazushige Tsunoda[2]
Masakazu Akahori[2]
Takeshi Iwata[2]
Yoshikazu Shimomura[1]

[1]Department of Ophthalmology, Kinki University Faculty of Medicine, Osaka-Sayama City, Osaka, Japan; [2]National Institute of Sensory Organs, National Hospital Organization Tokyo Medical Center, Tokyo, Japan

Background: We report our findings in two siblings with late-onset cone–rod dystrophy (CRD) with no visible macular degeneration.

Cases and methods: Case 1 was an 82-year-old man who first noticed a decrease in vision and color blindness in his early seventies. His mother and younger sister also had visual disturbances. His decimal visual acuity was 0.3 in the right eye and 0.2 in the left eye. Ophthalmoscopy showed normal fundi, and fluorescein angiography was also normal in both eyes. The photopic single flash and flicker eletroretinograms (ERGs) were severely attenuated and the scotopic ERGs were slightly reduced in both eyes. Case 2 was the 80-year-old younger sister of Case 1. She first noticed a decline in vision and photophobia in both eyes in her early seventies. Her decimal visual acuity was 0.4 in the right eye and 0.2 in the left eye. Ophthalmoscopy showed mottling of the retinal pigment epithelium in the midperiphery with no visible macular degeneration. The photopic single flash and flicker ERGs were severely attenuated, and the scotopic ERGs were slightly reduced in both eyes.

Conclusion: These siblings are the oldest reported cases of CRD with no visible macular degeneration. Thus, CRD should be considered in patients with reduced visual acuity, color blindness, and photophobia even if they are older than 70 years.

Keywords: cone–rod dystrophy, peripheral cone dystrophy, occult macular dystrophy, late onset, macular degeneration, negative ERG

Introduction

Cone–rod dystrophy (CRD) is an inherited retinal dystrophy that is characterized by reduced visual acuity, color blindness, and photophobia.[1–3] The age of onset generally ranges from the teens to the thirties,[2,3] and most patients with CRD have atrophic macular degeneration with a bull's eye lesion, or midperipheral degeneration in the late stages of the disease.[2,3] Patients with CRD can also have a central scotoma, and constriction of the peripheral visual fields at the end stages of the disease.[2,3] The cone-driven electroretinograms (ERGs) are attenuated even in the early stages, and this reduction is essential for making a diagnosis of CRD.[2,3]

Cases of atypical CRD, such as CRD with normal fundi,[4–7] occult macular dystrophy (OMD; Miyake disease),[8–11] peripheral cone dystrophy,[12–15] fundus albipunctatus associated with cone dystrophy,[16,17] and cone dystrophy with supernormal rod ERGs[18,19] have also been reported.

We present the clinical features of two siblings with CRD who had only mild fundus abnormalities. Their mother was also known to have visual difficulties, but was already dead at the time the two siblings were examined.

Correspondence: Kazuki Kuniyoshi
Department of Ophthalmology, Kinki University Faculty of Medicine, 377-2 Ohno-Higashi, Osaka-Sayama City, Osaka 589-8511, Japan
Tel +81 723 660 221
Fax +81 723 682 559
Email kazuki@med.kindai.ac.jp

Cases and methods

Our two cases were siblings who underwent ophthalmoscopy, visual acuity measurements, fundus fluorescein angiography (FA), Goldmann kinetic perimetry, Farnsworth D-15 test, Goldmann–Weekers dark adaptometry, full-field ERGs, multifocal ERGs (mfERGs), and optical coherence tomography (OCT). OCT images recorded from 24 age-matched normal subjects served as controls.

The ERGs and mfERGs were recorded according to the protocol recommended by the International Society for Clinical Electrophysiology of Vision. The mfERGs were recorded with the VERIS™ recording system (Electro-Diagnostic Imaging, Inc, Redwood, CA, USA). A Cirrus™ high-definition spectral-domain OCT instrument (Carl Zeiss Meditec AG, Jena, Germany) was used to obtain the OCT images.

Case reports

Case 1 was an 82-year-old man who first noticed a decrease in his vision and color vision in both eyes in his early seventies. His decimal best-corrected visual acuity (BCVA) at our initial examination was 0.3 oculus dexter (OD) with +3.25 diopters (D) and 0.2 oculus sinister (OS) with +3.25 D. His pupillary light reflexes and intraocular pressures were normal in both eyes. There was no history of the use of retinotoxic drugs. His cataracts were removed in both eyes at age 75; however, his vision was not improved.

Ophthalmoscopy showed that the fundus was normal in both eyes, and FA showed small hyperfluorescent spots at the parafoveal region of the left eye (Figure 1). Goldmann kinetic perimetry showed a central scotoma in both eyes (Figure 2), and Farnsworth D-15 test showed a tritan axis error. Goldmann–Weekers dark adaptometry revealed a slight elevation of the threshold in both eyes (Figure 3). The full-field scotopic ERGs elicited by both low- and high-intensity stimuli were slightly reduced. The scotopic b-wave elicited by a high-intensity stimulus was smaller than the a-wave, resulting in a negative-type ERG (Figure 4). On the other hand, photopic single-flash and 30 Hz flicker ERGs were severely attenuated in both eyes (Figure 4). The mfERGs were

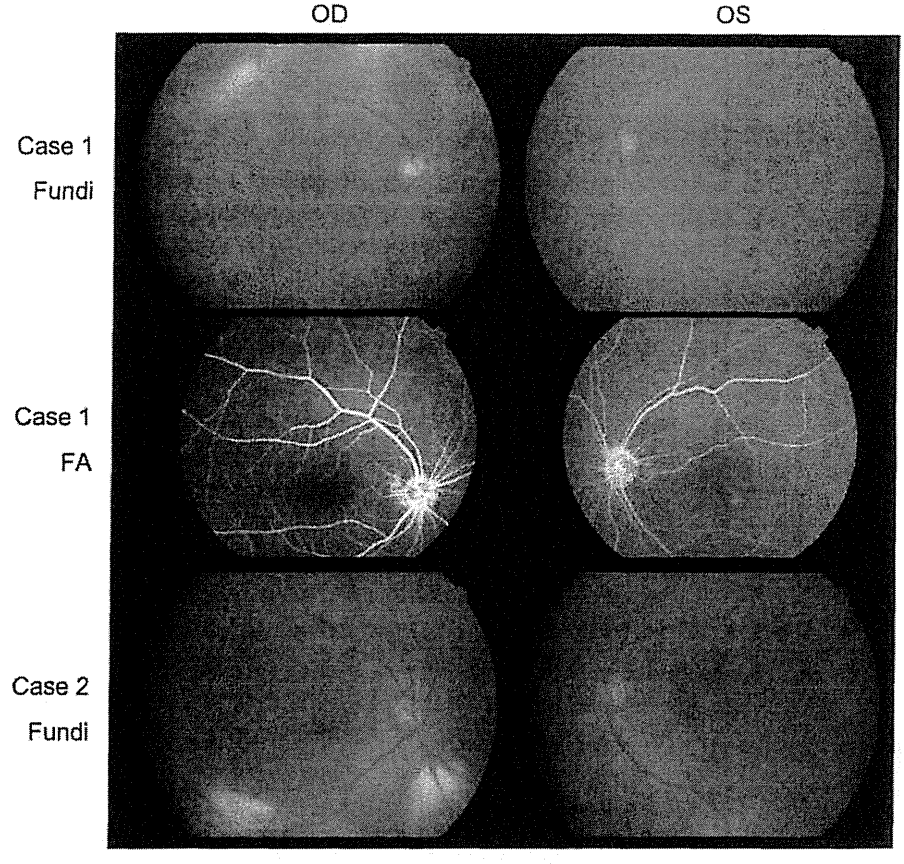

Figure 1 Fundus photographs (Fundi) and FA.
Abbreviations: OD, oculus dexter; OS, oculus sinister; FA, fluorescein fundus angiograms.

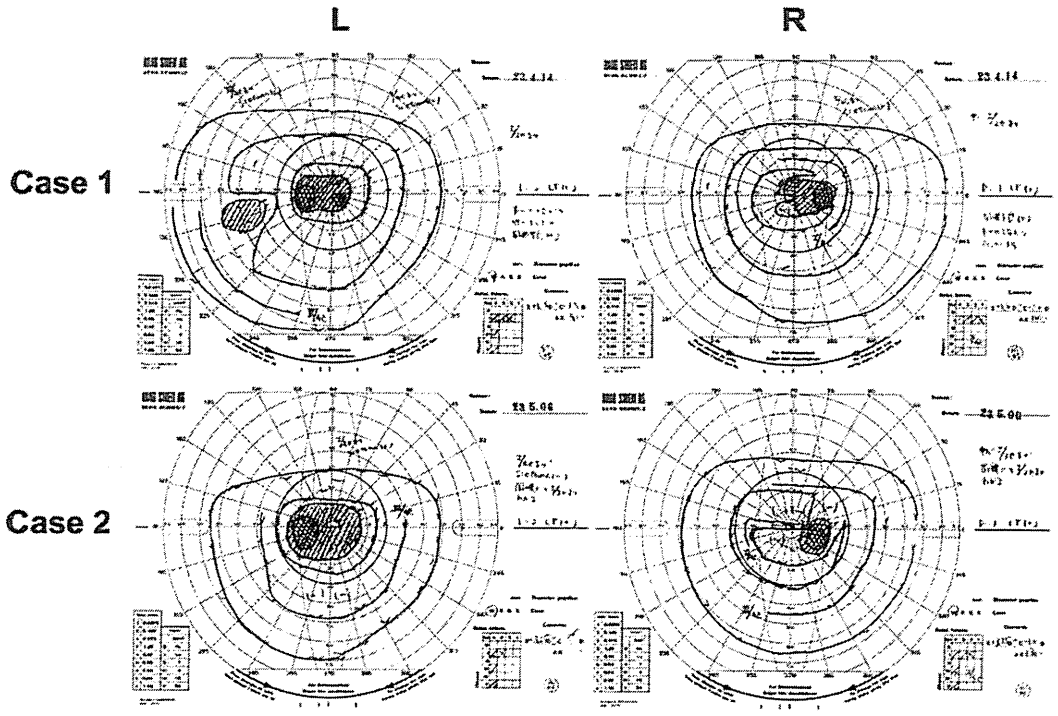

Figure 2 Results of Goldmann kinetic perimetry.
Abbreviations: L, left; R, right.

nonrecordable in the central area, but small responses were recorded in the midperiphery (Figure 5). The photoreceptor inner segment/outer segment junction line was indistinct in the OCT images (Figure 6). The thickness of the outer nuclear layer was 76 µm OD and 65 µm OS (normal mean 172 ± 17 µm) at the fovea, 65 µm OD and 43 µm OS (normal mean 128 ± 19 µm) at 0.5 mm superior to the fovea, and 65 µm OD and 54 µm OS (normal mean 135 ± 23 µm) at 0.5 mm inferior to the fovea. At 2 mm superior to the fovea, the thickness of the outer nuclear layer was 65 µm OD and 43 µm OS (normal mean 97 ± 13 µm), and at 2 mm inferior to the fovea it was 43 µm OD and 54 µm OS (normal

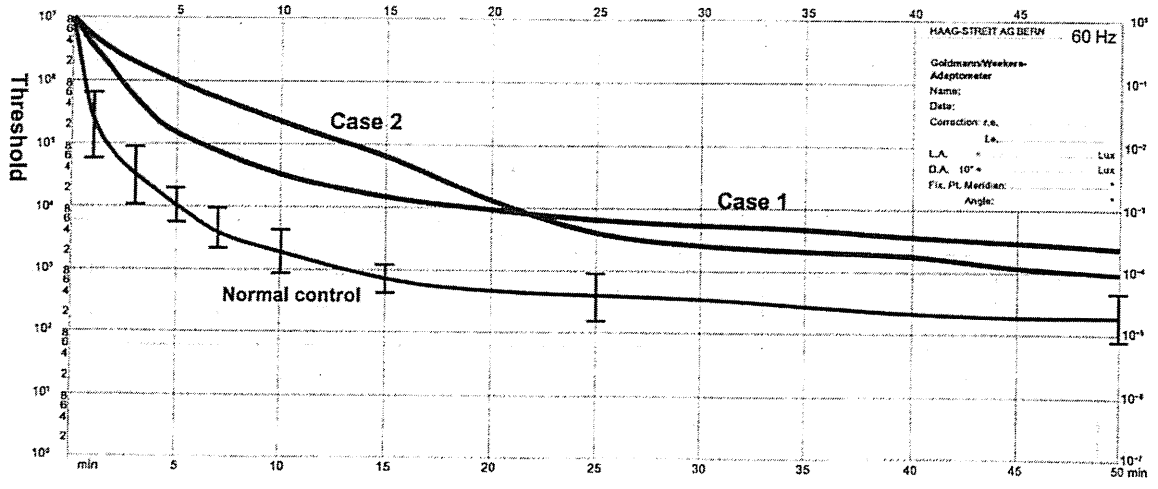

Figure 3 Results of Goldmann–Weekers dark adaptometry.
Note: The thin line indicates the average ± standard deviation isopter of normal controls.

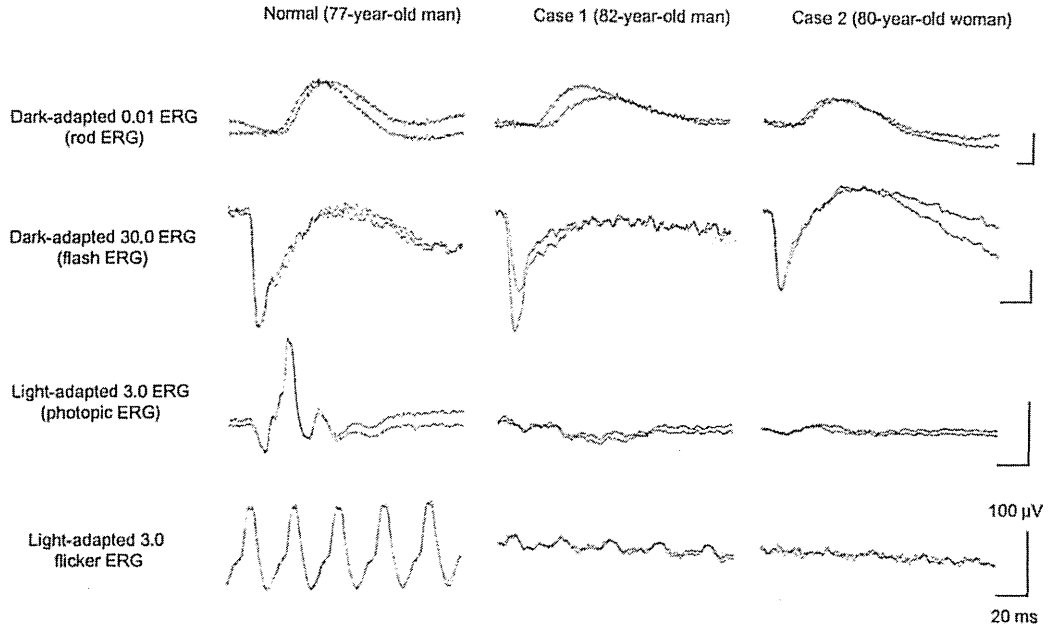

Figure 4 International Society for Clinical Electrophysiology of Vision-standard ERGs.
Note: The responses from both eyes are superimposed.
Abbreviation: ERG, electroretinography.

mean 88 ± 18 µm). Thus, the outer nuclear layer was thin, especially in the parafoveal region in both eyes (Figure 6). The thickness of the middle and inner layers of the retina were within normal limits.

Case 2 was the younger sister of case 1. She was 80 years old and had first noticed a decrease in her vision and photophobia in both eyes in her early seventies. Her cataract was removed in both eyes at age 76; however, her vision was not improved.

Our examination showed that her decimal BCVA was 0.4 OD with +0.25 D and 0.2 OS with +0.5 D. Her pupillary light reflexes and intraocular pressures were normal in both eyes. There was no history of retinotoxic drug use.

Her fundus was normal except for a slight mottling of the retinal pigment epithelium in the midperiphery. No macular degeneration was seen in either eye (Figure 1). FA was not performed because of her allergy to fluorescein sodium. Goldmann kinetic perimetry revealed a central scotoma in the left eye and a mild constriction of the visual fields in both eyes (Figure 2). Farnsworth D-15 test showed tritan axis errors in both eyes. Goldmann–Weekers dark adaptometry showed a slight elevation of the light threshold in both eyes (Figure 3). The full-field scotopic ERGs elicited by low-intensity stimuli were slightly reduced, and the scotopic high-intensity ERGs were normal, except the oscillatory potentials were reduced. The photopic single-flash and 30 Hz flicker ERGs were nonrecordable in both eyes (Figure 4). The mfERGs were nonrecordable in the right eye and reduced in the central and midperipheral areas of the left eye (Figure 5). OCT showed similar findings to her elder brother in the macular area (Figure 6). The photoreceptor inner segment/outer segment junction line was indistinct. The thickness of the outer nuclear layer was 130 µm OD and 129 µm OS (normal mean 172 ± 17 µm) at the fovea, 43 µm OD and 65 µm OS (normal mean 128 ± 19 µm) at 0.5 mm superior to the fovea, and 32 µm OD and 22 µm OS (normal mean 135 ± 23 µm) at 0.5 mm inferior to the fovea. At 2 mm superior to the fovea, the thickness of the outer nuclear layer was 65 µm OD and 76 µm OS (normal mean 97 ± 13 µm), and at 2 mm inferior to the fovea it was 65 µm OD and 43 µm OS (normal mean 88 ± 18 µm). Thus, the outer nuclear layer was thin, especially in the parafoveal region of both eyes (Figure 6).

Discussion

These two high-aged siblings, both in their eighties, had severely attenuated cone ERGs and mfERGs, and there was no evidence of visible macular abnormality. Case 1 had small hyperfluorescent spots in the fluorescein angiograms, and case 2 had mottling in the midperipheral fundus. Goldmann kinetic perimetry showed a central scotoma and reduced sensitivity in the area surrounding the scotoma in both patients. The mfERGs were nonrecordable in the foveal area, and only

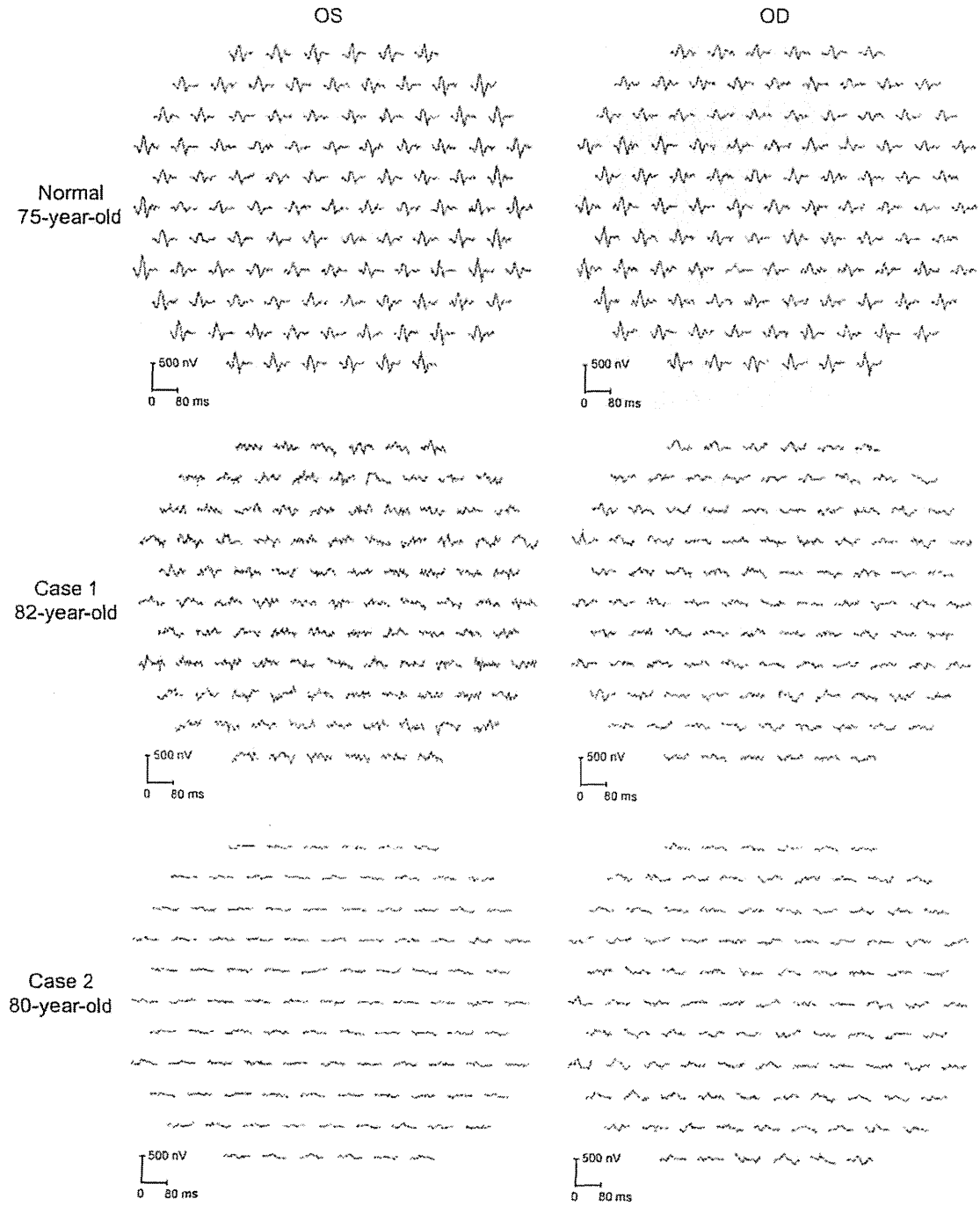

Figure 5 *Multifocal ERGs.*
Note: Responses were contaminated with much noise which was caused by photophobia.
Abbreviations: OS, oculus sinister; OD, oculus dexter; ERG, electroretinography.

very small responses were recorded in the midperiphery; these findings are consistent with results of the Goldmann kinetic perimetry.

We reviewed 497 CRD cases in 181 papers. Among these, 86 eyes in 43 patients in 20 papers were reported to have either normal fundus or only subtle fundus abnormalities (Figure 7).[4–7,20–35]

The vision of these cases is summarized in Figure 7, and the findings suggested that the vision in CRD cases with normal fundi is better than that in CRD cases with

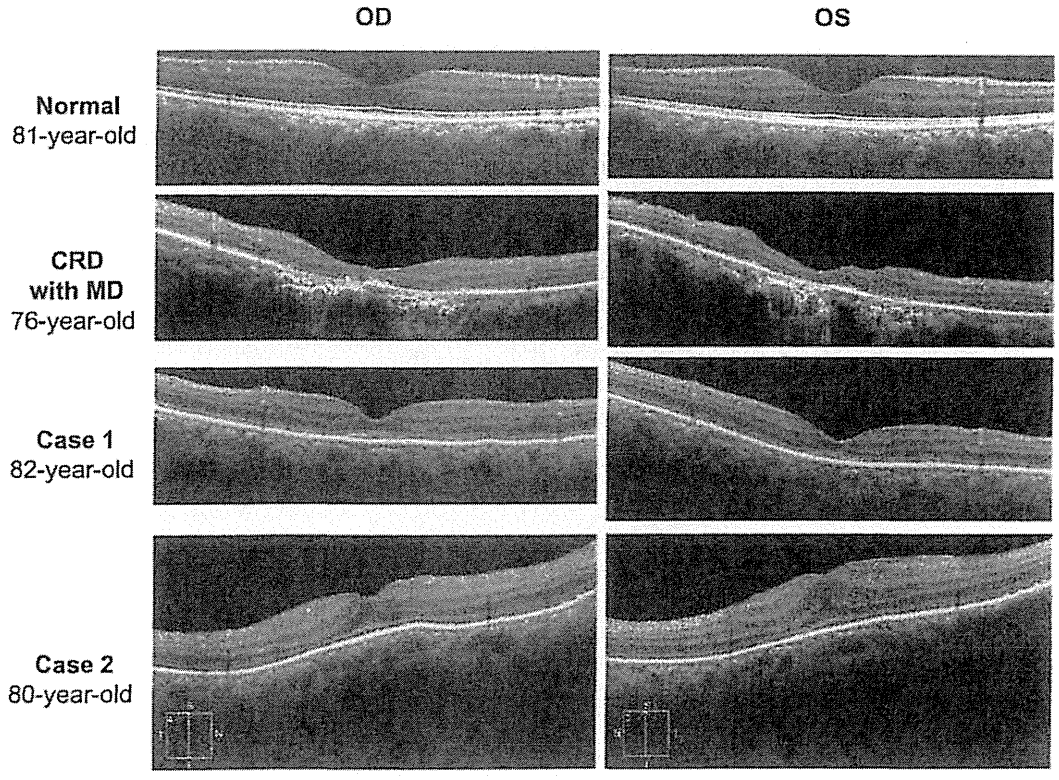

Figure 6 Results of optical coherence tomography.
Note: The photoreceptor inner segment/outer segment junction line is indistinct in the macular area.
Abbreviations: OD, oculus dexter; OS, oculus sinister; CRD, cone–rod dystrophy; MD, macular degeneration.

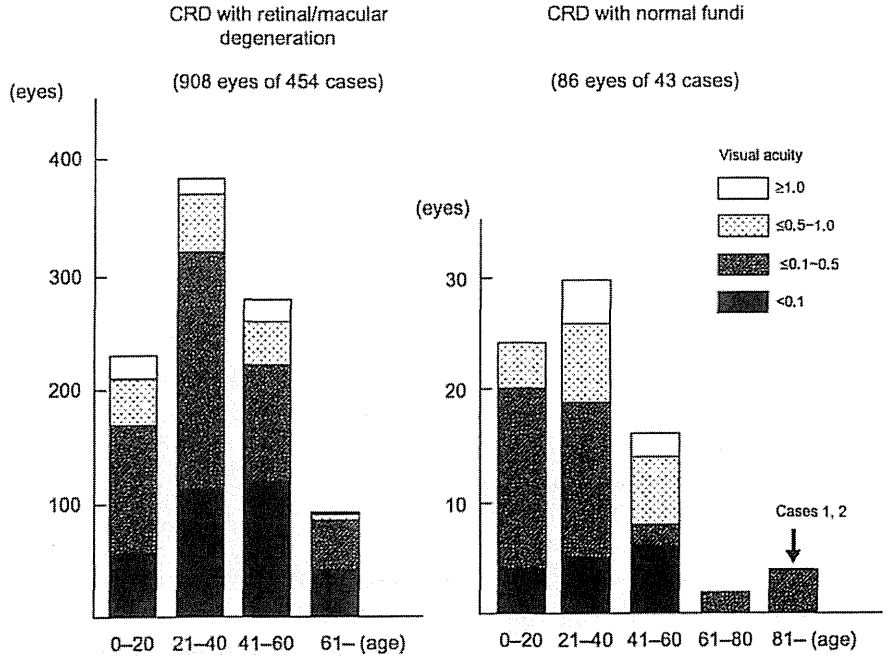

Figure 7 Age and visual acuity in cases with CRD in the past 181 papers published between 1963 and 2012.
Abbreviation: CRD, cone–rod dystrophy.

retinal/macular degeneration. Thirty-eight of 86 eyes (44%) with CRD and normal fundi had visual acuity better than 0.5, whereas 169 eyes of 908 eyes (19%) with retinal/macular degeneration had visual acuity better than 0.5.

Sixty-two of 86 eyes (72%) of the CRD cases with normal or subtle fundus abnormalities[4–7,20–35] had a family member with visible retinal degeneration, except the cases noted in studies by Ohba,[4] Rowe et al,[5] Miyake,[6] and Hayashi et al.[7] Ohba[4] reported on four CRD cases with normal fundi at ages 22 years, 23 years, 41 years, and 45 years. The patients' decimal BCVAs ranged from 0.1 to 0.07 in both eyes, and all were sporadic cases.[4] Rowe et al[5] reported four cases that were all sporadic and their ages were 55 years, 56 years, 60 years, and 68 years. Their decimal BCVAs ranged from 0.5 to 0.1 in both eyes.[5] Miyake[6] reported three cases of CRD with normal fundi from the same family whose ages were 32 years, 35 years, and 66 years. Their BCVAs were not reported. A sporadic, 53-year-old CRD case with normal fundi reported by Hayashi et al[7] had BCVAs of 0.1 OD and 0.7 OS.

CRD cases with normal fundi and no family history of retinal degeneration have a late onset, with an average age of 46 years and an average BCVA of 0.24. In comparison, the CRD cases with retinal or macular degeneration had an average age at onset of 23 years and the average BCVA was 0.09. The two siblings in our study had a very late onset with a positive family history and normal fundi. Their BCVAs after cataract removal ranged from 0.4 to 0.2 in both eyes, which are beyond the normal range reported,[36] and are comparable to the CRD cases with normal fundi and no family history of retinal degeneration.[4–7]

OMD is a kind of cone dystrophy with a normal fundus appearance.[8–11] Recently, a point mutation was found in the *RP1L1* gene in patients with autosomal-dominant OMD.[10] The ERG findings on our siblings are different from these cases of OMD because of the almost nonrecordable full-field cone response in our cases, which is due to diffuse cone dysfunction in these cases.

Peripheral cone dystrophy (or peripheral cone disease) is another kind of cone dystrophy that is characterized by cone dysfunction in the midperiphery to the periphery.[12–15] All of the past cases were reported as peripheral cone dystrophy and all had normal fundi. The gene mutation causing this cone dystrophy has not been identified. The results of mfERGs in our two cases were different from past cases of peripheral cone dystrophy because the mfERGs from the macula were nonrecordable. However, the two siblings in our study were probably at an advanced stage of the peripheral cone dystrophy because their outer nuclear layer at the fovea was well preserved compared with that of patients with cone dystrophy and a bull's eye lesion (Figure 6).

Several gene mutations have been identified in cases of CRD. Mutations of the *CRX* gene,[26,27,32,37–40] the *GUCY2D* gene,[29,33,35,41] the *GUCA1A* gene,[42] and *peripherin/RDS* gene[43] have been found in cases of autosomal-dominant CRD. Mutations of the *ABCA4* gene,[44] *CNGB3* gene,[28] and *KCNV2* gene,[19,30,31,34] have been reported for the autosomal-recessive cases of CRD. Mutations of the *CACNA1F* gene[45] and *RPGR* gene[46] have been detected in X-linked recessive cases of CRD.

Mutations of the *CRX* gene,[26,27,32] as well as the *GUCY2D*,[29,33,35] *KCNV2*,[30,31,34] and *CNGB3*[28] genes might be the cause of CRD in eyes with normal or mild fundus abnormalities. Cases with mutations in the *CRX* gene have diverse phenotypes ranging from Leber's congenital amaurosis[39,47] to CRD with normal fundi.[26,27,32] Sohocki et al[39] suggested that these varied phenotypes in patients with the *CRX*-gene mutations were due to deletion or point mutations in the gene. Deletion mutations in this gene would result in late-onset and mild CRD.[39] Our cases are similar to CRD cases with mutations in the *CRX* gene.

Swain et al[38] and Itabashi et al[40] reported CRD cases caused by a *CRX* gene mutation that had negative ERGs. Case 1 in our study had a reduced b-wave in the high-intensity ERGs that resembled the ERGs reported by Swain et al[38] and Itabashi et al.[40]

Mutations in other genes such as the *GUCY2D* gene,[26,27,32] *KCNV2* gene[30,31,34] and *CNGB3* gene[28] have also been reported to cause CRD with normal fundi; however, these patients were relatively young and some had supernormal rod responses, unlike our cases.

We investigated the gene in the siblings presented in our study using next-generation sequencing. However, detection of the causative mutation in these siblings was difficult because most of their family members, including their parents, were already deceased.

In summary, we report our findings in two siblings with late-onset CRD. Ophthalmoscopy showed that the macula was essentially normal in both cases. The scotopic ERGs were slightly reduced, but the photopic ERGs were nonrecordable. We recommended that older patients, >45 years of age, who had good vision earlier in their lives but had developed reduced vision, color vision abnormalities, and photophobia be examined by electroretinography to rule out CRD.

Acknowledgments

This research was supported in part by research grants from the Ministry of Health, Labor and Welfare, Japan, and Japan Society for the Promotion of Science, Japan.

Disclosure

The authors report no conflicts of interest in this work.

References

1. Steinmetz RD, Ogle KN, Rucker CW. Some physiologic considerations of hereditary macular degeneration. *Am J Ophthalmol.* 1956;42(4 Pt 2):304–319.
2. Krill AE, Deutman AF, Fishman M. The cone degenerations. *Doc Ophthalmol.* 1973;35(1):1–80.
3. Thiadens AA, Phan TM, Zekveld-Vroon RC, et al; Writing Committee for the Cone Disorders Study Group Consortium. Clinical course, genetic etiology, and visual outcome in cone and cone-rod dystrophy. *Ophthalmology.* 2012;119(4):819–826.
4. Ohba N. Progressive cone dystrophy; four cases of unusual form. *Jpn J Ophthalmol.* 1974;18(1):50–69.
5. Rowe SE, Trobe JD, Sieving PA. Idiopathic photoreceptor dysfunction causes unexplained visual acuity loss in later adulthood. *Ophthalmology.* 1990;97(12):1632–1637.
6. Miyake Y. Phenotypes of cone dysfunction syndrome. *Folia Ophthalmol Jpn.* 2000;51(8):725–733. Japanese.
7. Hayashi K, Yamada H, Wakakura M. A case of late-onset cone-rod dystrophy (CRD) which lacked ophthalmoscopic findings and diagnosed by electrophysiological examination. *Neuro-Ophthalmol Japan.* 2005;22(2):246–252. Japanese.
8. Miyake Y, Ichikawa K, Shiose Y, Kawase Y. Hereditary macular dystrophy without visible fundus abnormality. *Am J Ophthalmol.* 1989;108(3):292–299.
9. Miyake Y, Horiguchi M, Tomita N, et al. Occult macular dystrophy. *Am J Ophthalmol.* 1996;122(5):644–653.
10. Akahori M, Tsunoda K, Miyake Y, et al. Dominant mutations in *RP1L1* are responsible for occult macular dystrophy. *Am J Hum Genet.* 2010;87(3):424–429.
11. Tsunoda K, Usui T, Hatase T, et al. Clinical characteristics of occult macular dystrophy in family with mutation of *RP1L1* gene. *Retina.* 2012;32(6):1135–1147.
12. Pinckers A, Deutman AF. Peripheral cone disease. *Ophthalmologica.* 1977;174(3):145–150.
13. Kondo M, Miyake Y, Kondo N, Ueno S, Takakuwa H, Terasaki H. Peripheral cone dystrophy: a variant of cone dystrophy with predominant dysfunction in the peripheral cone system. *Ophthalmology.* 2004;111(4):732–739.
14. Okuno T, Oku H, Kurimoto T, Oono S, Ikeda T. Peripheral cone dystrophy in an elderly man. *Clin Experiment Ophthalmol.* 2008;36(9):897–899.
15. Baek J, Lee HK, Kim US. Spectral domain optical coherence tomography findings in bilateral peripheral cone dystrophy. *Doc Ophthalmol.* 2013;126(3):247–251.
16. Miyake Y, Shiroyama N, Sugita S, Horiguchi M, Yagasaki K. Fundus albipunctatus associated with cone dystrophy. *Br J Ophthalmol.* 1992;76(6):375–379.
17. Nakamura M, Hotta Y, Tanikawa A, Terasaki H, Miyake Y. A high association with cone dystrophy in Fundus albipunctatus caused by mutations of the *RDH5* gene. *Invest Ophthalmol Vis Sci.* 2000;41(12):3925–3932.
18. Gouras P, Eggers HM, MacKay CJ. Cone dystrophy, nyctalopia, and supernormal rod responses. A new retinal degeneration. *Arch Ophthalmol.* 1983;101(5):718–724.
19. Wu H, Cowing JA, Michaelides M, et al. Mutations in the gene *KCNV2* encoding a voltage-gated potassium channel subunit cause "cone dystrophy with supernormal rod electroretinogram" in humans. *Am J Hum Genet.* 2006;79(3):574–579.
20. Goodman G, Ripps H, Siegel IM. Cone dysfunction syndromes. *Arch Ophthalmol.* 1963;70:214–231.
21. Berson EL, Gouras P, Gunkel RD. Progressive cone degeneration, dominantly inherited. *Arch Ophthalmol.* 1968;80(1):77–83.
22. François J, de Rouck A, Verriest G, de Laey JJ, Cambie E. Progressive generalized cone dysfunction. *Ophthalmologica.* 1974;169(4):255–284.
23. Ripps H, Noble KG, Greenstein VC, Siegel IM, Carr RE. Progressive cone dystrophy. *Ophthalmology.* 1987;94(11):1401–1409.
24. van Schooneveld MJ, Went LN, Oosterhuis JA. Dominant cone dystrophy starting with blue cone involvement. *Br J Ophthalmol.* 1991;75(6):332–336.
25. Iijima H, Yamaguchi S, Kogure S, Hosaka O, Shibutani T. Electroretinogram in cone dystrophy. *Jpn J Ophthalmol.* 1991;35(4):453–466.
26. Jacobson SG, Cideciyan AV, Huang Y, et al. Retinal degenerations with truncation mutations in the cone-rod homeobox (*CRX*) gene. *Invest Ophthalmol Vis Sci.* 1998;39(12):2417–2426.
27. Tzekov RT, Sohocki MM, Daiger SP, Birch DG. Visual phenotype in patients with Arg41Gln and ala196+1 bp mutations in the *CRX* gene. *Ophthalmic Genet.* 2000;21(2):89–99.
28. Michaelides M, Aligianis IA, Ainsworth JR, et al. Progressive cone dystrophy associated with mutation in *CNGB3*. *Invest Ophthalmol Vis Sci.* 2004;45(6):1975–1982.
29. Smith M, Whittock N, Searle A, Croft M, Brewer C, Cole M. Phenotype of autosomal dominant cone-rod dystrophy due to the R838C mutation of the *GUCY2D* gene encoding retinal guanylate cyclase-1. *Eye (Lond).* 2007;21(9):1220–1225.
30. Wissinger B, Dangel S, Jägle H, et al. Cone dystrophy with supernormal rod response is strictly associated with mutations in *KCNV2*. *Invest Ophthalmol Vis Sci.* 2008;49(2):751–757.
31. Ben Salah S, Kamei S, Sénéchal A, et al. Novel *KCNV2* mutations in cone dystrophy with supernormal rod electroretinogram. *Am J Ophthalmol.* 2008;145(6):1099–1106.
32. Kitiratschky VB, Nagy D, Zabel T, et al. Cone and cone-rod dystrophy segregating in the same pedigree due to the same novel *CRX* gene mutation. *Br J Ophthalmol.* 2008;92(8):1086–1091.
33. Kitiratschky VB, Wilke R, Renner AB, et al. Mutation analysis identifies *GUCY2D* as the major gene responsible for autosomal dominant progressive cone degeneration. *Invest Ophthalmol Vis Sci.* 2008;49(11):5015–5023.
34. Robson AG, Webster AR, Michaelides M, et al. "Cone dystrophy with supernormal rod electroretinogram": a comprehensive genotype/phenotype study including fundus autofluorescence and extensive electrophysiology. *Retina (Philadelphia, Pa).* 2010;30(1):51–62.
35. Garcia-Hoyos M, Auz-Alexandre CL, Almoguera B, et al. Mutation analysis at codon 838 of the *guanylate cyclase 2D* gene in Spanish families with autosomal dominant cone, cone-rod, and macular dystrophies. *Mol Vis.* 2011;17:1103–1109.
36. Sjöstrand J, Laatikainen L, Hirvelä H, Popovic Z, Jonsson R. The decline in visual acuity in elderly people with healthy eyes or eyes with early age-related maculopathy in two Scandinavian population samples. *Acta Ophthalmol.* 2011;89(2):116–123.
37. Freund CL, Gregory-Evans CY, Furukawa T, et al. Cone-rod dystrophy due to mutations in a novel photoreceptor-specific homeobox gene (*CRX*) essential for maintenance of the photoreceptor. *Cell.* 1997;91(4):543–553.
38. Swain PK, Chen S, Wang QL, et al. Mutations in the cone-rod homeobox gene are associated with the cone-rod dystrophy photoreceptor degeneration. *Neuron.* 1997;19(6):1329–1336.
39. Sohocki MM, Sullivan LS, Mintz-Hittner HA, et al. A range of clinical phenotypes associated with mutations in *CRX*, a photoreceptor transcription-factor gene. *Am J Hum Genet.* 1998;63(5):1307–1315.

40. Itabashi T, Wada Y, Sato H, Kawamura M, Shiono T, Tamai M. Novel 615delC mutation in the CRX gene in a Japanese family with cone-rod dystrophy. *Am J Ophthalmol*. 2004;138(5):876–877.
41. Kelsell RE, Gregory-Evans K, Payne AM, et al. Mutations in the retinal guanylate cyclase (*RETGC-1*) gene in dominant cone-rod dystrophy. *Hum Mol Genet*. 1998;7(7):1179–1184.
42. Payne AM, Downes SM, Bessant DA, et al. A mutation in guanylate cyclase activator 1A (GUCA1A) in an autosomal dominant cone dystrophy pedigree mapping to a new locus on chromosome 6p21.1. *Hum Mol Genet*. 1998;7(2):273–277.
43. Nakazawa M, Kikawa E, Chida Y, Wada Y, Shiono T, Tamai M. Autosomal dominant cone-rod dystrophy associated with mutations in codon 244 (Asn244His) and codon 184 (Tyr184Ser) of the peripherin/RDS gene. *Arch Ophthalmol*. 1996;114(1):72–78.
44. Cremers FP, van de Pol DJ, van Driel M, et al. Autosomal recessive retinitis pigmentosa and cone-rod dystrophy caused by splice site mutations in the Stargardt's disease gene *ABCR*. *Hum Mol Genet*. 1998;7(3):355–362.
45. Jalkanen R, Mäntyjärvi M, Tobias R, et al. X linked cone-rod dystrophy, CORDX3, is caused by a mutation in the *CACNA1F* gene. *J Med Genet*. 2006;43(8):699–704.
46. Demirci FY, Rigatti BW, Wen G, et al. X-linked cone-rod dystrophy (locus *CODI*): identification of mutations in *RPGR* exon ORF15. *Am J Hum Genet*. 2002;70(4):1049–1053.
47. Freund CL, Wang QL, Chen S, et al. De novo mutations in the *CRX* homeobox gene associated with Leber congenital amaurosis. *Nat Genet*. 1998;18(4):311–312.

Molecular Vision 2013; 19:1580-1590 <http://www.molvis.org/molvis/v19/1580>
Received 1 April 2013 | Accepted 15 July 2013 | Published 20 July 2013

Molecular characteristics of four Japanese cases with *KCNV2* retinopathy: Report of novel disease-causing variants

Kaoru Fujinami,[1,2] Kazushige Tsunoda,[1] Natsuko Nakamura,[1] Yu Kato,[1] Toru Noda,[1] Kei Shinoda,[3] Kaoru Tomita,[4] Tetsuhisa Hatase,[5] Tomoaki Usui,[6] Masakazu Akahori,[1] Takeshi Itabashi,[1] Takeshi Iwata,[1] Yoko Ozawa,[2] Kazuo Tsubota,[2] Yozo Miyake[1,7]

[1]National Institute of Sensory Organs, National Tokyo Medical Center, Tokyo, Japan; [2]Department of Ophthalmology, Keio University, School of Medicine, Tokyo, Japan; [3]School of Medicine, Teikyo University, Tokyo, Japan; [4]Heiwa Ganka Clinic, Tokyo, Japan; [5]Graduate School of Medical and Dental Sciences, Niigata University, Niigata, Japan; [6]Akiba Eye Clinic, Niigata, Japan; [7]Aichi Medical University, Aichi, Japan

Purpose: To describe the molecular characteristics of four Japanese patients with cone dystrophy with supernormal rod responses (CDSRR).

Methods: Four individuals with a clinical and electrophysiological diagnosis of CDSRR were ascertained. The pathognomonic findings of the full-field electroretinograms (ERGs) included a decrease in the rod responses, a square-shaped a-wave, an excessive increase in the b-wave in the bright flash responses, and decreased cone-derived responses. Mutational screening of the coding regions and flanking intronic sequences of the potassium channel, subfamily V, member 2 (*KCNV2*) gene was performed with bidirectional sequencing. The segregation of each allele was confirmed by screening other family members. Subsequent in silico analyses of the mutational consequences for protein function were performed.

Results: There were two siblings from one family and one case in each of the two families. One family had a consanguineous marriage. Mutational screening revealed compound heterozygosity for the two alleles, p.C177R and p.G461R, in three patients, and homozygosity for complex alleles, p.R27H and p.R206P, in one patient from the consanguineous family. There were three putative novel variants, p.R27H, p.C177R, and p.R206P. The four variants in the families with *KCNV2* were highly conserved in other species. In silico analyses predicted that all of the missense variants would alter protein function.

Conclusions: Biallelic disease-causing variants were identified in four Japanese patients with CDSRR suggesting that the pathognomonic electrophysiological features are helpful in making a molecular diagnosis of *KCNV2*. Three novel variants were identified, and we conclude that there may be a distinct spectrum of *KCNV2* alleles in the Japanese population.

Patients with cone dystrophy and supernormal rod electroretinograms (ERGs) were first reported in 1983, and the abnormality in the ERGs indicated a progressive degeneration of the cone photoreceptors associated with unique rod system abnormalities [1]. More detailed characteristics of this rare, autosomal recessive condition were reported in later studies, and the disease was named cone dystrophy with supernormal rod responses (CDSRR; MIM #610356) [2-8].

Most cases with CDSRR typically present in the first two decades of life with reduced visual acuity, abnormal color vision, and photophobia [8-11]. Night blindness is a later feature of the disorder [8]. The fundus appearance is variable, with some having a normal peripheral retina and a range of macular abnormalities [8-10]. The pattern of the autofluorescence (AF) images is also variable: Young cases have either a normal pattern or small parafoveal ring enhancements, while older cases have a narrow high-signal annulus that can encircle a central atrophic area of the retinal pigment epithelium (RPE) [6,12]. Recently, spectral domain optical coherence tomography (SD-OCT) and adaptive optics scanning laser ophthalmoscope (AOSLO) studies have described morphological changes of the fovea even at the early stages [10,13,14].

The electrophysiological findings are pathognomonic of CDSRR, and they assist in its early diagnosis [3,5,8-12,15-17]. The light-adapted ERGs are usually delayed and decreased in keeping with a generalized cone system dysfunction. There is also a unique rod system abnormality; the dark-adapted ERGs elicited by dim flashes are markedly decreased and delayed, and increasing the flash intensity results in an excessive increase in the b-wave amplitude accompanied by a shortening of the peak time of the b-wave [8,9,11]. A square-shaped a-wave trough of the dark-adapted bright flash ERGs is also a characteristic feature of this disorder [9,11].

Correspondence to: Kazushige Tsunoda, Laboratory of Visual Physiology, National Institute of Sensory Organs, 2-5-1 Higashigaoka, Meguro-ku, Tokyo 152-8902, Japan; Phone: +81334110111; FAX: +81334110185; email: tsunodakazushige@kankakuki.go.jp

CDSRR has been shown to be caused by mutations in the potassium channel, subfamily V, member 2 (*KCNV2*) gene (MIM# 607,604), which encodes a voltage-gated potassium channel subunit, Kv8.2 [18]. This silent subunit is expressed in rod and cone photoreceptors [18-20], and is thought to assemble with other K^+ channel subunits such as KCNB1, KCNC1, and KCNF1. These subunits form functional heteromeric channels with altered properties that have a narrowed membrane potential for activation and slow inactivation kinetics [19]. Eventually, these kinetic properties result in transient hyperpolarization overshoots on rapid changes in the inward currents [19]. A deficiency of Kv8.2 by a mutation in *KCNV2* may affect the characteristics of the I_{kx} as first described in amphibian photoreceptors [21]. This deficiency may influence the photoreceptor membrane potential. However, the underlying mechanisms that fully explain the clinical features of CDSRR are still not determined.

More than 50 different disease-causing variants in *KCNV2* have been reported: small insertion and deletion changes or large deletions that constitute a protein truncation and single nucleotide changes with amino acid substitutions [9,10,13,14,16,18,22,23]. Three small case series describe the clinical features of CDSRR in East Asians [3,5,15]; however, molecular genetic studies of these populations have not been published. Thus, the purpose of this study was to determine the molecular genetic characteristics from the clinical and electrophysiological findings of four Japanese patients who were diagnosed with CDSRR.

METHODS

Subjects: Four subjects who were diagnosed with CDSRR from the clinical and electrophysiological findings were ascertained at the National Institute of Sensory Organs, National Tokyo Medical Center, Tokyo, Japan and Niigata University, Niigata, Japan. The natural history of these four patients has been partially reported recently [24]. The procedures used were approved by the ethics committee of each institution, and all procedures were performed in accordance with the principles of the Declaration of Helsinki. Informed consent was obtained from all experimental subjects for all procedures.

Clinical assessment: A complete medical history was obtained, and a comprehensive ophthalmological examination was performed on all patients. The photophobia and night blindness episode was obtained on direct questioning. The clinical assessments included measurements of the best-corrected visual acuity (BCVA), dilated ophthalmoscopy, color fundus photography, AF imaging, OCT, and electrophysiological recordings. AF images were obtained with the HRA 2 confocal scanning laser ophthalmoscope (Heidelberg Engineering, Heidelberg, Germany; excitation light, 488 nm; barrier filter, 500 nm; field of view, 30×30°) [25]. The OCT images were obtained with SD-OCT (Cirrus HD-OCT, versions 4.5 and 5.1; Carl Zeiss Meditec, Dublin, CA) [26].

Electrophysiological assessments: Full-field ERGs were recorded from the four patients with the minimum standard protocol of the International Society for Clinical Electrophysiology of Vision (ISCEV) [27]. The ERG examination included the following: (i) dark adapted dim flash 0.01 $cd \cdot s \cdot m^{-2}$ (DA 0.01), (ii) dark adapted bright flash 30.0 $cd \cdot s \cdot m^{-2}$ (DA 30.0), (iii) light adapted 3.0 $cd \cdot s \cdot m^{-2}$ at 2 Hz (LA 3.0), and (iv) light adapted 3.0 $cd \cdot s \cdot m^{-2}$ 30 Hz flicker ERG (LA 3.0 30Hz). The extended protocol included the recording of the dark-adapted ERGs elicited by stimulus intensities of 0.001 $cd \cdot s \cdot m^{-2}$, 0.01 $cd \cdot s \cdot m^{-2}$, 0.3 $cd \cdot s \cdot m^{-2}$, 3.0 $cd \cdot s \cdot m^{-2}$, and 30.0 $cd \cdot s \cdot m^{-2}$. Two of the four patients were also recorded with the extended protocol. An excessive or disproportionate increase in the dark adapted b-wave with increasing flash intensity was assessed in these two patients, according to the previous report [9].

Mutational screening: After informed consent was obtained, blood samples were collected in EDTA tubes from each subject, and the DNA was extracted with a DNA extraction kit (QIAamp DNA Blood Maxi Kit; Qiagen, Venlo, the Netherlands). All exons and exon–intron boundaries were amplified with polymerase chain reaction (PCR), and the primer sequences used are shown in Table 1. PCR was performed with 20 µl volume containing 0.5 Unit Taq polymerase (PrimeStar GXL DNA polymerase, Takara, Tokyo, Japan). The sequence was determined based on the dideoxy terminator method using an ABI PRISM 3100×l Genetic Analyzer (Applied Biosystems, Foster City, CA) according to the manufacturer's protocol. The SeqScape Software version 2.5 (Applied Biosystems) was used to analyze the sequence alignment. Bidirectional Sanger sequencing was also performed in other family members of the proband, to confirm the segregation of the alleles.

Molecular genetic analyses: All of the missense variants identified were analyzed using two software prediction programs, Sorting Intolerant from Tolerance (SIFT) and PolyPhen2 [28,29]. The predicted effects on splicing of all missense variants were assessed with the Human Splicing finder program version 2.4.1. The allele frequency of each variant was estimated with the Exome Variant Server (NHLBI Exome Sequencing Project, Seattle, WA). A multiple sequence alignment program for DNA or proteins, the Clustal Omega, was applied to confirm an evolutionary conservation. Likely non-disease-causing variants (polymorphisms)

Table 1. Primer Sequences and Conditions for *KCNV2* Mutational Screening.

Primer	Sequence (5'–3')	Product size (bp)	PCR annealing (°C)
E1aF	AGGACCTGAGAAGGGGCAGCT	831	71
E1aR	TCCAGGAGGCGGAGGAACTCT		
E1bF	CCCTGCTGTCCACGCTGAATG	799	71
E1bR	CAGCGTGGGTAAGGTGGGTCA		
E1cF	AAGATCCAGCACGAGCTGCGC	841	65
E1cR	ATGGATGTCAAAAGTGGTGGA		
E2aF	AGCTTCTGTTCTTTTCATGAC	624	63
E2aR	GTCTCATAGTTGCTCTGTGTT		

bp = base pairs.

were also analyzed with the same protocol applied to likely disease-causing variants.

RESULTS

The demographic features of the four individuals from three families with CDSRR are summarized in Table 2. There were two siblings (patients 1 and 2) in one family and one case in each of the two families (patients 3 and 4). The pedigree of each family is shown in Figure 1, and a consanguineous marriage was present in family 3.

Clinical findings: The age of the patient at the time of the examination was 23, 17, 21, and 17 years with the age of disease onset at 9, 5, 3, and 2 years (Table 2). Three patients complained of photophobia (patients 1, 2, and 4), and all four patients had night blindness. Patient 4 had had mild nystagmus since age 2 years. The decimal BCVA of the four patients ranged from 0.08 to 0.8, and the BCVA of patients 1 and 2 was better than 0.7 in each eye.

The findings obtained from the color fundus photographs, AF images, and SD-OCT images are summarized in Figure 1 and Table 2. The fundus photographs showed mottling of the RPE at the macula in all four patients with subtle patchy granular flecks at the macula in patient 3. A ring enhancement of the AF signal was detected in the AF images of all four patients; three subjects had it centered on the fovea (patients 1, 2, and 3), and one had it at the parafovea (patient 4). In patient 3, the ring enhancement at the fovea was surrounded by patchy granular foci of the high AF signal at the macula.

SD-OCT demonstrated abnormalities in the outer retinal layers in all four patients. The cone outer segment tip line was absent in the macular area in all patients. The photoreceptor inner and outer segment junction line was discontinuous at the fovea in patients 3 and 4, and thinning of the outer retina was detected at the fovea in all four patients.

Electrophysiological assessments: The electrophysiological findings are summarized in Table 3, and the ERGs are shown in Figure 2. The full-field ERGs were recorded with the minimum ISCEV standard from patients 2 and 3, and extended protocol full-field ERGs including the dark-adapted ERGs elicited by an intensity series were obtained from patients 1 and 4.

The dark adapted b-wave amplitude elicited by a stimulus intensity 0.01 (DA0.01) was delayed and decreased in patients 3 and 4, but was normal but delayed in patient 1. The responses for DA0.01 were undetectable in patient 2. An excessive increase in the b-wave for the extended protocol was found in two patients, 1 and 4. In addition, the a-wave was square-shaped with a supernormal b-wave elicited by stimulus intensity 30.0 (DA 30.0) in all four patients. The photopic ERGs (LA 3.0 and LA 3.0 30Hz) were decreased in all four patients (Table 3 and Figure 2).

Molecular genetics: The molecular genetic findings are summarized in Table 2 and Appendix 1. Likely disease-causing variants in *KCNV2* were identified in all four patients. The four likely disease-causing variants were p.Arg27His, p.Cys177Arg, p.Arg206Pro, and p.Gly461Arg (Appendix 1), and two likely non-disease-causing variants (polymorphisms) were p.Gly61Gly and p.Ala265Ala (Appendix 2). The segregation of each allele was confirmed by screening of other family members for all these variants.

Detailed molecular results including in silico analysis to assist in predicting the pathogenicity of the four disease-causing variants identified are shown in Appendix 1. All of the four likely disease-causing variants were single nucleotide changes with one amino acid substitution (missense), i.e., p.Arg27His, p.Cys177Arg, p.Arg206Pro, and p.Gly461Arg. Compound heterozygosity for the two alleles, p.Cys177Arg and p.Gly461Arg, in patients 1, 2, and 3 and homozygosity for the complex alleles, p.Arg27His and p.Arg206Pro, in patient

Table 2. Summary of demographics, clinical findings and molecular status for four Japanese patients with *KCNV2*-retinopathy

Pt, FM, gender	Onset of disease, age at examination (years)	VA		Fundus		AF		OCT		Mutation status
		RE	LE	RPE mottling	Subtle patchy granular flecks	Ring enhancement	Patchy granular foci of high signal	Absence of COST	Deficit of IS/OS	
1, 1, F	9, 23	0.7	0.8	Macula	ND	Fovea	ND	Fovea	ND	Compund heterozygous [c.529 T>C, p.Cys177Arg]; [c.1381G>A, p.Gly461Arg]
2, 1, M	5,17	0.7	0.7	Macula	ND	Fovea	ND	Fovea	ND	Compund heterozygous [c.529 T>C, p.Cys177Arg]; [c.1381G>A, p.Gly461Arg]
3, 2, F	3,21	0.1	0.1	Macula	Macula	Fovea	Macuala	Macula	Fovea	Compund heterozygous [c.529 T>C, p.Cys177Arg]; [c.1381G>A, p.Gly461Arg]
4, 3, F	2, 17	0.1	0.08	Macula	ND	Para-fovea	ND	Macula	Fovea	Complex homozygous [c.80 G>A, p.Arg27His]; [c.617 G>C, p.Arg206Pro]

Pt = Patient; FM = family number; VA = logMAR visual acuity; RE = right eye; LE = left eye; RPE = retinal pigment epithelium; AF = autofluorescence; COST = cone outer segment tip line; IS/OS = photoreceptor inner and outer segment junction; ND = not detected. The affected area of each finding is based on the color fundus photographs, AF images, and the OCT images in each column.

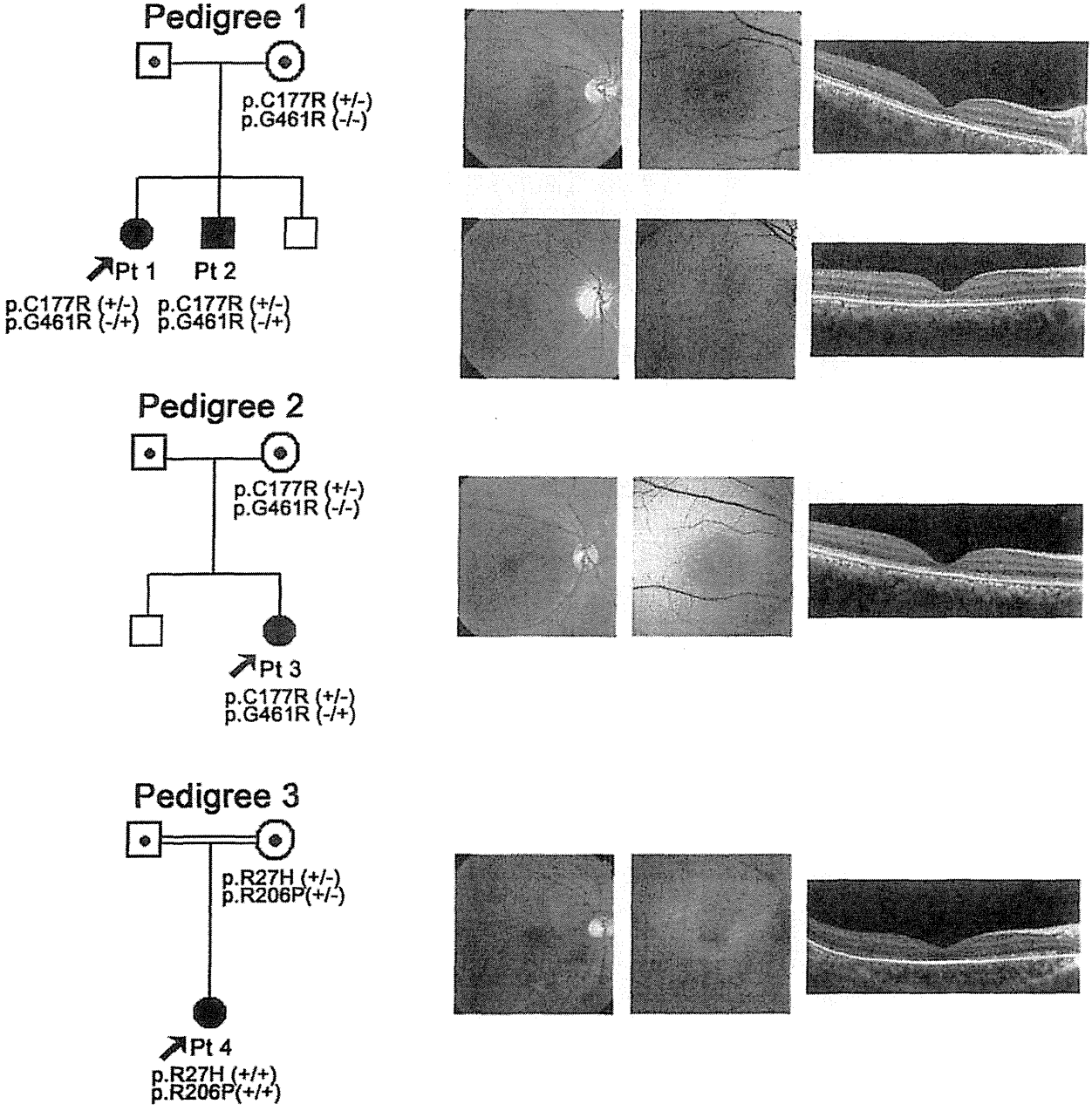

Figure 1. Pedigree and retinal imaging of each patient with potassium channel, subfamily V, member 2 retinopathy. Pedigrees with molecular status of the three families with potassium channel, subfamily V, member 2 (*KCNV2*) retinopathy are shown on the left. Retinal images including color fundus photographs, autofluorescence images, and spectral domain optical coherence tomography are presented on the right. Images of patient 1 (top row), patient 2 (second row from top), patient 3 (third row from top), and patient 4 (bottom row) are shown.

4 were revealed by the segregation analyses. The p.Gly461Arg variant has been reported, and the p.Arg27His, p.Cys177Arg, and p.Arg206Pro variants are putative novel. In silico analysis revealed an "intolerant" protein function or a "probably or possibly damaged" protein but no effect on splicing in the three putative novel variants (SIFT, Poplyphen2, and Human Splicing finder; Appendix 1). The reported missense variant, p.Gly461Arg, with possibly affecting splicing was detected in six out of 13,006 individuals of the Exome Variant Server; the three novel variants, p.Arg27His, p.Cys177Arg, and